JACS
JOURNAL OF THE AMERICAN CHEMICAL SOCIETY
Article
pubs.acs.org/JACS

Tailored Design of Multiple Nanoarchitectures in Metal-Cyanide Hybrid Coordination Polymers

Ming Hu,*[,†,‡] Alexei A. Belik,[‡] Masataka Imura,[‡] and Yusuke Yamauchi*[,‡,§,∥]

[†]International Center for Young Scientists (ICYS), National Institute for Materials Science (NIMS), 1-1 Namiki, Tsukuba, Ibaraki 305-0044, Japan

[‡]World Premier International (WPI) Research Center for Materials Nanoarchitectonics (MANA), National Institute for Materials Science (NIMS), 1-1 Namiki, Tsukuba, Ibaraki 305-0044, Japan

[§]Faculty of Science and Engineering, Waseda University, 3-4-1 Okubo, Shinjuku, Tokyo 169-8555, Japan

[∥]Precursory Research for Embryonic Science and Technology (PRESTO), Japan Science and Technology Agency (JST), 4-1-8 Honcho, Kawaguchi, Saitama 332-0012, Japan

Supporting Information

ABSTRACT: Recently, coordination polymers (CPs) with nanoscale porosity and unique property have demonstrated great potential in many applications. Encouraged by significant progress in the controlled synthesis of nanomaterials, such as metals and semiconductors, the morphologically controlled synthesis of CPs has been considered a potential way to further enhance the inherent properties and develop new functions. In particular, hollow-based CPs are promising nanoarchitectures that can bring several properties derived from crystalline thin shells and interior cavities. Here we demonstrate an exquisite construction method to synthesize CPs with multiple hollow-based nanoarchitectures. Through step-by-step CP crystal growth and subsequent etching processes, various types of CPs with shell-in-shell, yolk-shell, and yolk-double-shell hollow structures can be synthesized for the first time. This type of nanoarchitecture is powerful for the exploration of alternative properties of CPs. The resultant hollow-based nanoarchitectures significantly increase gas adsorption and bring out interesting magnetic properties.

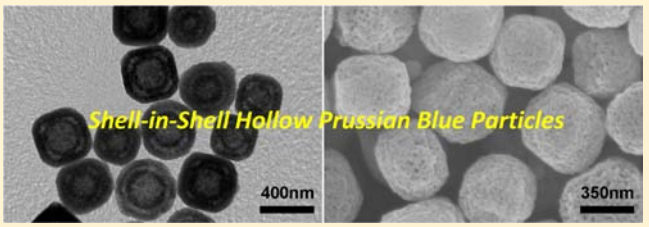

1. INTRODUCTION

Microporous coordination polymers (CPs), including porous metal−organic frameworks (MOFs) or porous coordination polymers (PCPs), are crystalline inorganic−organic hybrid materials with high surface areas and uniform micropores.[1−5] Their great potentials have been realized in separation, catalysis, gas storage, and sensing.[6−11] Recently, nanostructure control has been proved to be a promising way to enhance performance or explore new properties;[12−17] this has encouraged us to fabricate microporous CPs with exquisite nanostructures for a fundamental understanding of the relationship between the nanostructures and the properties of microporous CPs.[18−26]

In particular, hollow-based nanostructures containing enclosed large cavities and thin shells have attracted wide interest because of their unique influence on optical, magnetic, and mechanical properties, catalytic activity, storage capability, and permeability of materials.[27−35] Success in the preparation of sophisticated hollow structures, such as shell-in-shell, yolk-shell, and more complicated hollow structures with multiple components, demonstrates that nanoscale fabrication can be greatly controlled, leading to advanced materials that can be utilized to solve problems related to energy, the environment, and life science.[36−41] Inspired by these aspects, it is of great interest to synthesize hollow-based microporous CPs and explore their properties.

Pioneering attempts have demonstrated that monoshell hollow microporous CPs showed good permeability and large amounts of guest molecule uptake,[42−47] thereby offering great motivation to researchers to explore this topic more deeply and broadly. However, a main drawback has been the difficulty in the preparation of hollow microporous CPs with more complicated exquisite structures. Current methods can only succeed in monoshell hollow microporous CPs with a single component but cannot meet the needs for the synthesis of various hollow-based microporous CPs, for example, multiple-shell and yolk-shell nanostructures with multiple components.

To realize various hollow-based microporous CPs, here we establish a new synthetic concept by step-by-step CP crystal growth and subsequent etching processes. To demonstrate this concept, we selected Prussian Blue ($Fe_4[Fe(CN)_6]_3{\cdot}xH_2O$, PB) and its analogues, which are important metal−cyanide hybrid coordination polymers with high potential in wide applications,[48−56] as our model materials. The general chemical formula of the PB analogues can be described as

Received: September 30, 2012
Published: December 27, 2012

   dx.doi.org/10.1021/ja3096703 | J. Am. Chem. Soc. 2013, 135, 384−391

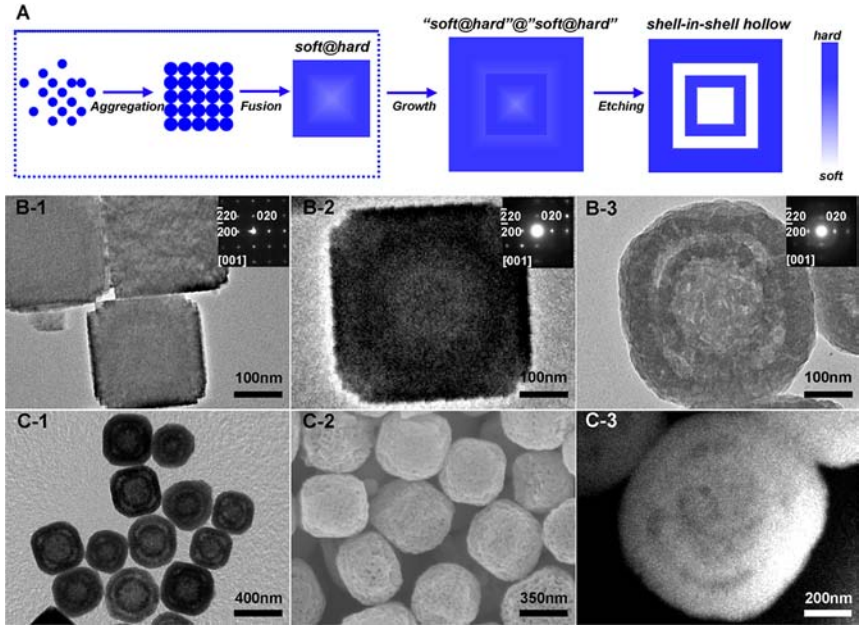

Figure 1. (A) Schematic illustration for making shell-in-shell FeFe hollow particles. TEM images of (B-1) FeFe particles as the starting seeds; (B-2) 'soft@hard'@'soft@hard' FeFe particle grown on the seed; and (B-3) shell-in-shell hollow FeFe particle after chemical etching. (C-1) Low-magnified TEM image of shell-in-shell hollow FeFe particles after chemical etching. (C-2) SEM image of shell-in-shell hollow FeFe particles after chemical etching. (C-3) HAADF-STEM image of a shell-in-shell hollow FeFe particle.

$A_lM_n[M'_m(CN)_6)]\cdot xH_2O$ (A represents alkali metal, and M and M′ represent transition metals). Hereafter, we abbreviate the PB analogues as MM′ on the basis of their transition metals (e.g., PB itself is FeFe). For most PB analogues, the crystal structures and lattice constants are close to each other. Therefore, it is possible to make the PB analogues with heterogeneous structures by epitaxial deposition (i.e., seed-mediated growth).[57−59] The PB analogues can slowly disassociate in a hot HCl solution.[43] Owing to the different chemical stability by location, subsequent chemical etching provides different etching rates, thereby forming complicated hollow structures. Thus, through careful design of the sequential crystal growth and subsequent etching of the PB analogues, various kinds of hollow-based microporous CP nanomaterials can be synthesized. These hollow-based microporous CP nanomaterials exhibit distinct properties, compared to solid microporous CP particles without hollow interiors.

2. EXPERIMENTAL SECTION

2.1. Synthesis of Shell-in-Shell Hollow FeFe Particles. PVP (3.00 g) and $K_3[Fe(CN)_6]\cdot 3H_2O$ (132 mg) were added to a 0.1 M HCl solution (40.0 mL) under magnetic stirring. After 30 min of stirring, a clear solution was obtained. The vial was then placed into an electric oven and heated at 80 °C for 20 h. After aging, the precipitates were collected by centrifugation and washed in distilled water and ethanol several times. After drying at room temperature for 12 h, the resulting powder was obtained and used as the seed for the next step. The seed (10.0 mg), PVP (3.00 g), and $K_3[Fe(CN)_6]\cdot 3H_2O$ (132 mg) were then added to a 0.01 M HCl solution (40 mL) under magnetic stirring. After 30 min of stirring, a clear solution was obtained. The vial was then placed into an electric oven and heated at 80 °C for 20 h. After aging, the precipitates were collected by centrifugation and washed in distilled water and ethanol several times. After drying at room temperature for 12 h, PB nanocubes with 200 nm in particle size were obtained and later used as soft@hard FeFe seeds (Figure 1). The obtained soft@hard FeFe PB seeds (10.0 mg), PVP (3.00 g), and $K_3[Fe(CN)_6]\cdot 3H_2O$ (132 mg) were added to a 0.01 M HCl solution (40 mL) under magnetic stirring. After 30 min of stirring, a clear solution was obtained. The vial was then placed into an electric oven and heated at 80 °C for 20 h. After aging, the precipitates were collected by centrifugation and washed in distilled water and ethanol several times. After drying at room temperature for 12 h, PB nanocubes with 390 nm in particle size were obtained, which were 'soft@hard'@'soft@hard' FeFe particles as shown in Figure 1.

The obtained 'soft@hard'@'soft@hard' FeFe particles (20 mg) were immersed in 20 mL of 1 M HCl solution in a Teflon vessel under magnetic stirring. After 1 h, the vessel was transferred into a stainless autoclave and heated at 135 °C for 3 h in an electric oven. (Caution! The −CN group may be converted to HCN gas in hot acidic solution. So, the preparation should be always carried out in fume hood.) After aging, the precipitates were collected by centrifugation and washed in distilled water and ethanol several times. After drying at room temperature for 12 h, shell-in-shell hollow FeFe particles were obtained.

2.2. Synthesis of PB Analogues with a Yolk-Shell Structure. *2.2.1. FeFe@CoFe Particles with a Yolk-Shell Structure.* PVP (3.00 g) and $K_3[Fe(CN)_6]\cdot 3H_2O$ (132 mg) were added to a 0.1 M HCl solution (40.0 mL) under magnetic stirring. After 30 min of stirring, a clear solution was obtained. The vial was then placed into an electric oven and heated at 80 °C for 20 h. After aging, the precipitates were collected by centrifugation and washed in distilled water and ethanol several times. After drying at room temperature for 12 h, a powder was obtained and used as the seed for the next step.

In the following step, the obtained seed (10 mg), cobalt chloride (77.9 mg), and sodium citrate (397.1 mg) were dissolved in 20 mL water to form a blue dispersion in bottle A. In the meantime, $K_3[Fe(CN)_6]$ (132 mg) was dissolved into 20 mL water to form a clear solution in bottle B. The solution in bottles A and B was then mixed under magnetic stirring until the mixture became clear. The obtained solution was aged for 24 h until the purple precipitates were collected by centrifugation. After extensive washing in water and ethanol, the purple precipitates were dried at room temperature. The obtained purple powders were FeFe@CoFe particles with a core-shell structure.

For creating a yolk−shell structure, 20 mg of FeFe@CoFe particles with a core-shell structure was immersed in a 2 M HCl solution (20 mL) under magnetic stirring. After 1 h, the vessel was transferred into a stainless autoclave and heated at 120 °C for 3 h in an electric oven.

dx.doi.org/10.1021/ja3096703 | J. Am. Chem. Soc. 2013, 135, 384−391

(Caution! The −CN group may be converted to HCN gas in hot acidic solution. So, the preparation should be always carried out in fume hood.) After aging, the precipitates were collected by centrifugation and washed in distilled water and ethanol several times. After drying at room temperature for 12 h, FeFe@CoFe particles with a yolk-shell structure were obtained.

2.2.2. NiCo@CoFe Particles with a Yolk−Shell Structure. Nickel chloride (142.6 mg) and sodium citrate (264.7 mg) were dissolved in 20 mL water to form clear solution A. In the meantime, $K_3[Co(CN)_6]$ (133 mg) was dissolved in 20 mL water to form clear solution B. Solutions A and B were then mixed under magnetic stirring until the mixture became clear. The obtained solution was aged for 10 h until pale-blue precipitates were collected by centrifugation. After extensive washing in water and ethanol, the precipitates were dried at room temperature. After drying at room temperature for 12 h, a powder was obtained and used as the seed for the next step.

In the following step, the obtained seed (10 mg), cobalt chloride (77.9 mg), and sodium citrate (397.1 mg) were dissolved in 20 mL water to form a dispersion in bottle A. In the meantime, $K_3[Fe(CN)_6]$ (132 mg) was dissolved into 20 mL water to form a clear solution in bottle B. The solution in bottles A and B was mixed under magnetic stirring until the mixture became clear. The obtained solution was aged for 24 h until the purple precipitates were collected by centrifugation. After extensive washing in water and ethanol, the purple precipitates were dried at room temperature. The obtained purple powders were NiCo@CoFe particles with a core-shell structure.

For creating the yolk-shell structure, 20 mg of NiCo@CoFe particles with a core-shell structure was immersed in a 2 M HCl solution (20 mL) under magnetic stirring. After 1 h, the vessel was transferred into a stainless autoclave and heated at 120 °C for 3 h in an electric oven. (Caution! The −CN group may be converted to HCN gas in hot acidic solution. So, the preparation should be always carried out in fume hood.) After aging, the precipitates were collected by centrifugation and washed in distilled water and ethanol several times. After drying at room temperature for 12 h, NiCo@CoFe particles with a yolk-shell structure were obtained.

2.3. Synthesis of PB Analogues with a Yolk-Double-Shell Structure. PVP (3.00 g) and $K_3[Fe(CN)_6]\cdot 3H_2O$ (132 mg) were added to a 0.1 M HCl solution (40.0 mL) under magnetic stirring. After 30 min of stirring, a clear solution was obtained. Then, the vial was placed into an electric oven and heated at 80 °C for 20 h. After aging, the precipitates were collected by centrifugation and washed in distilled water and ethanol several times. After drying at room temperature for 12 h, the resulting powder was obtained and used as a seed for the next step. Then, the seed (10.0 mg), PVP (3.00 g), and $K_3[Fe(CN)_6]\cdot 3H_2O$ (132 mg) were added to a 0.01 M HCl solution (40 mL) under magnetic stirring. After 30 min of stirring, a clear solution was obtained. The vial was then placed into an electric oven and heated at 80 °C for 20 h. After aging, the precipitates were collected by centrifugation and washed in distilled water and ethanol several times. After drying at room temperature for 12 h, FeFe nanocubes with 200 nm in particle size were obtained. For creating a hollow cavity, FeFe nanocubes (20.0 mg) and PVP (100 mg) were added to a 1.0 M HCl solution (20 mL) in a Teflon vessel under magnetic stirring. After 2 h, the vessel was transferred into a stainless autoclave and heated at 135 °C for 3 h in an electric oven. (Caution! The −CN group may be converted to HCN gas in hot acidic solution. So, the preparation should be always carried out in fume hood.) After aging, the precipitates were collected by centrifugation and washed in distilled water and ethanol several times. After drying at room temperature for 12 h, hollow FeFe nanocubes were obtained.

In the following step, the obtained hollow FeFe nanocubes (10 mg), nickel chloride (142.6 mg), and sodium citrate (264.7 mg) were dissolved in 20 mL water to form a dispersion in bottle A. In the meantime, $K_3[Co(CN)_6]$ (133 mg) was dissolved into 20 mL water to form a clear solution in bottle B. Then, the solution in bottles A and B was mixed under magnetic stirring until the mixture became clear. The obtained solution was aged for 24 h until the precipitates were collected by centrifugation. After extensive washing in water and ethanol, the precipitates were dried at room temperature. The obtained yolk-double-shell structure was described as NiCo@(-FeFe@NiCo), where NiCo and FeFe@NiCo represent a core and a double-shell structure, respectively.

2.4. Characterization. SEM images were taken with a Hitachi SU8000 scanning microscope at an accelerating voltage of 5 kV. The TEM observation was performed by using a JEM-2100F TEM system operated at 200 kV. Wide-angle powder X-ray diffraction (XRD) patterns were obtained with a Rigaku RINT 2500X diffractometer using monochromated Cu Kα radiation (40 kV, 40 mA) at a scanning rate of 1° min^{-1}. Nitrogen adsorption−desorption data were obtained by the use of a Quantachrome Autosorb Automated Gas Sorption System at 77 K.

3. RESULTS AND DISCUSSION

3.1. Shell-in-Shell Hollow FeFe Particles. As the first example, we prepared shell-in-shell hollow FeFe ($Fe_4[Fe(CN)_6]_3\cdot xH_2O$) particles by epitaxial growth and subsequent controlled etching, as illustrated in Figure 1A. It has been generally known that the FeFe colloidal nanocubes are formed by self-aggregation of tiny nanocrystals that lead to defects within the nanocubes.[60] The distribution of defects varies by different locations owing to the in-uniform fusion of tiny nanocrystals. Basically, dissolution and recrystallization effect can help to reduce the defects. Fewer defects are expected to present in the shell part owing to the fact that dissolution and recrystallization can occur more easily in shell parts. Therefore, specific defects distribution can be expected inside the FeFe colloidal nanocubes. For each nanocubes, the inside core has more defects than outside shell, which is like a core-shell structure. Considering more defects can result in weaker stability, we name the part with more defects as "soft" part (brighter blue parts), while the part with fewer defects as "hard" part (darker blue parts). Therefore, FeFe colloidal nanocubes are considered to have a "soft@hard" structure. By further using these "soft@hard" particles as seeds, another layer of FeFe was coated on the seeds. The additional layer will also have a "soft@hard" structure thus lead to "soft@hard"@"soft@hard" particles. When these particles were immersed into an acidic solution, H^+ ions could go through the defects and work inside the whole particles. Depending on the density of the defects, the etching rates of different parts varied. The parts with more defects were etched more quickly. Therefore, the 'soft' parts could be removed, while the 'hard' parts could be preserved, resulting in shell-in-shell hollow structures.

A transmission electron microscopy (TEM) image of the "soft@hard" FeFe colloidal nanocubes is presented in Figure 1B-1. Step-like edges and periodic diffraction spots indicate that the particles are an oriented aggregation of nanoparticles. Darker shells and brighter cores suggest the "soft@hard" structure. After using these particles as seeds, larger particles were obtained. Periodic diffraction spots obtained from a whole particle confirmed that epitaxial growth happened on the seeds (Figure 1B-2). The step-like surface on the nanocubes suggests that the particles still contain defects, similarly to the starting FeFe seeds. The specific locations of darker and brighter parts indicate that they are "soft@hard"@"soft@hard". These large particles were then dispersed in a hot HCl solution for etching. Figure 1B-3 shows that the final products were hollow particles with cavities. Two shells were contained in a single particle, which resembles a concentric shell-in-shell structure. Interestingly, both the outside and the inner shell share the same crystallographic orientation, as suggested by ED patterns taken from the whole particle. To fully demonstrate the yield of particles, a low-magnified TEM image is shown in Figure 1C-1.

dx.doi.org/10.1021/ja3096703 | J. Am. Chem. Soc. 2013, 135, 384−391

Most of the particles (>98%) are of shell-in-shell structures. The three-dimensional morphology of these particles was further checked by scanning electron microscopy (SEM). All of the particles were quasicubic and with rough shells (Figure 1C-2). High-angle annular dark field scanning TEM (HAADF-STEM) image further confirmed that the inside shell was also of quasicubic shape, similarly to an outside shell (Figure 1C-3). The purity of the product was assessed by powder X-ray diffraction (XRD) (Figure S1). These shell-in-shell hollow particles were a pure face-center-cubic structure with an $Fm\bar{3}m$ system (JCPDS card 73-0687), similar to the solid particles shown in Figure 1B-2. The much sharper diffraction peaks of shell-in-shell particles suggest that these particles are of better crystallinity than the solid precursors, due to the removal of the 'soft' part. Elemental analysis confirmed that the composition of the FeFe particles is close to $Fe_4[Fe(CN)_6]_3{\cdot}14H_2O$.

Figure 2A illustrates the N_2 gas adsorption−desorption isotherms of shell-in-shell hollow FeFe particles and solid FeFe

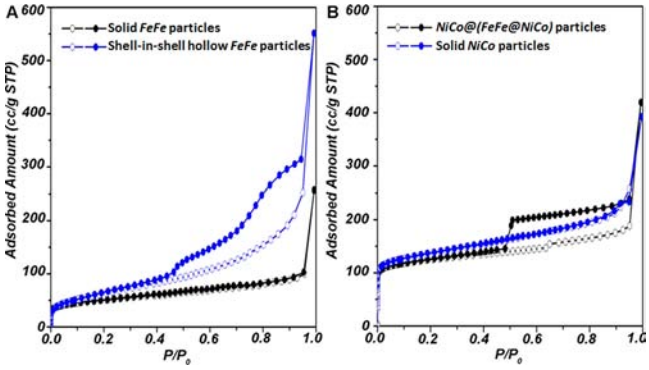

Figure 2. N_2 gas sorption isotherms taken at 77 K. (A) Shell-in-shell hollow FeFe particles and solid FeFe particles and (B) NiCo@(-FeFe@NiCo) particles with a yolk-double-shell structure and solid NiCo particles.

particles. For both samples, a drastic increase at low relative pressure ($P/P_0 < 0.01$) was observed, indicating the presence of inherent micropores of FeFe. However, a significant difference was observed in the range of $P/P_0 = 0.4-1.0$. A larger amount of N_2 gas was adsorbed by shell-in-shell hollow FeFe particles than in solid ones. This means that the shell-in-shell hollow particles contained mesopores that were formed during the etching process. Indeed, the mesopores were randomly formed in the shell region, and their sizes were widely distributed from a few nanometers to 20 nm, as observed in the high-resolution SEM image (Figure S2). Thanks to the additional meso-porosity, the surface area of shell-in-shell hollow particles increased up to 229 m^2/g, a much higher value than that of solid particles. Furthermore, a large hysteresis loop was detected for shell-in-shell hollow particles, while no loop could be observed for solid FeFe ones. The complicated shell-in-shell structure probably slowed down the release rate of the N_2 molecules, which are adsorbed inside the hollow cavity. Owing to the double-shell structures existing in each particle, the desorption process of N_2 molecules was hindered twice, resulting in the two steps observed in the desorption isotherm.

3.2. PB Analogues with a Yolk-Shell Structure. The above concept is applicable to other heterocomposites with different components that can result in new materials with alternative or multiple functions.[57−59,61] The first step is to prepare PB analogue composites with a core-shell structure. Here, FeFe nanoparticles were used as the starting seeds. The CoFe ($Co_3[Fe(CN)_6]_2{\cdot}xH_2O$) was then deposited on the surface of the seeds. To deposit the CoFe analogue layer, sodium citrate was used as an additive. Sodium citrate can interact with free metal ions dissolved in aqueous solution, thereby decreasing the coordination speed between metal ions and the targeted ligands. Due to the low crystallization rate, the second layers were uniformly coated on the FeFe seeds.[62−64] The TEM image shows FeFe@CoFe core-shell particles. As clearly observed in Figure 3A-1, the different contrast between

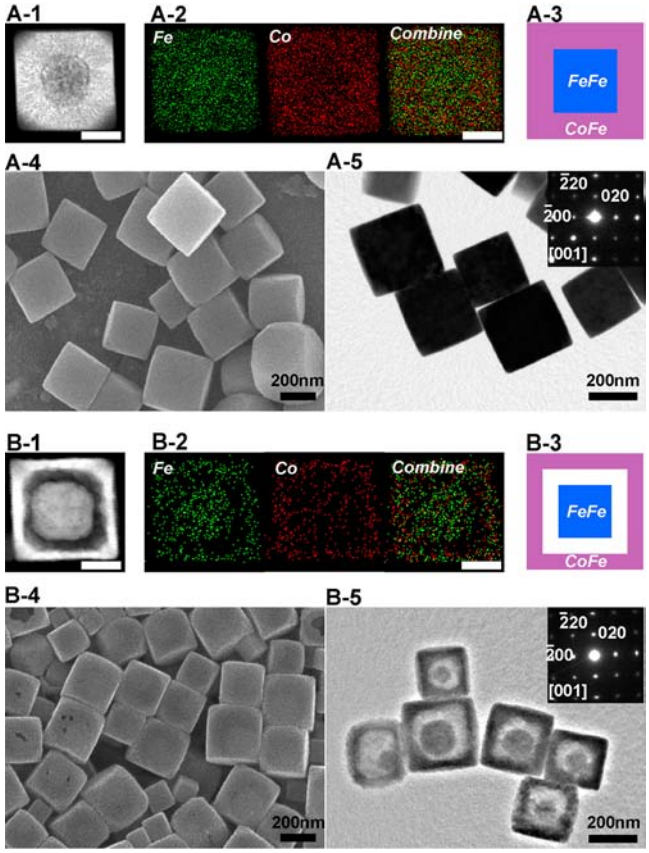

Figure 3. (A-1) HAADF-STEM image of a core-shell FeFe@CoFe particle. (A-2) Elemental mapping of a core-shell FeFe@CoFe particle. (A-3) Structure of a core-shell particle. The scale bars are 100 nm. (A-4) SEM image of core-shell FeFe@CoFe particles. (A-5) Low-magnified TEM image of core-shell FeFe@CoFe particles and ED patterns taken from a single particle. (B-1) HAADF-STEM image of a yolk-shell FeFe@CoFe particle. (B-2) Elemental mapping of a yolk-shell FeFe@CoFe particle. (B-3) Structure of a core-shell particle. The scale bars are 100 nm. (B-4) SEM image of yolk-shell FeFe@CoFe particles. (B-5) Low-magnified TEM image of yolk-shell FeFe@CoFe particles and ED patterns taken from a single particle.

the inner center and outer parts indicates the formation of a core-shell structure. The metal of FeFe PB is only Fe, while the metals of the CoFe PB analogue are Co and Fe. Considering this point, nanoscale elemental mapping is a powerful tool to confirm the core-shell structure. Elemental mapping analysis taken from the particle (Figure 3**A-2**) revealed the center parts that contain more iron than the edge parts, which further supports the formation of the FeFe@CoFe core-shell structure (Figure 3A-3). The obtained core-shell particles have a cubic morphology (Figures 3A-4,5). Selected area ED patterns (inset of Figure 3A-5) taken from a whole core-shell particle showing

dx.doi.org/10.1021/ja3096703 | J. Am. Chem. Soc. 2013, 135, 384−391

a single crystalline state, indicating that the shell parts epitaxially grew on the core part due to the similar crystal structures between the FeFe and the CoFe PB analogues. From the wide-angle XRD profile (Figure S3, profile A), it was confirmed that these core-shell particles had a pure face-center-cubic structure, which is identical to the typical structure of the CoFe (JCPDS card 78448). Considering the slight difference in the crystal constants between FeFe and CoFe PB analogues, their peak positions should be a little different. However, only the CoFe PB analogue as the outer shell was detected. Due to large shell thickness, the FeFe core became undetectable by normal X-ray analysis.

The FeFe and CoFe regions show a different stability in acid solution. The obtained FeFe@CoFe core-shell particles were immersed into a hydrochloride solution to create a hollow cavity. Figure 3B-1 revealed that the core-shell particles were converted to hollow-based structures with a yolk-shell structure. The core and shell were totally separated after the etching, which typically belongs to a yolk-shell structure. Elemental mapping (Figure 3B-2) suggests that the yolk and shell inherit the initial compositions of FeFe@CoFe core-shell particles (in which the core is FeFe and the shell is CoFe) (Figure 3B-3). The low-magnified SEM and TEM images showed the high yield of the yolk-shell particles with cube shapes, and more than 90% particles were yolk-shell structures (Figures 3B-4,5). Surprisingly, the inner yolk particles possessed a similar crystallographic orientation to the outer shell parts. The periodic diffraction spots in the selected area ED patterns taken from a single particle demonstrating a single crystallographic orientation. Different from the XRD patterns of the starting FeFe@CoFe core-shell particles, XRD patterns of the obtained FeFe@CoFe yolk-shell particles could be assigned as two phases that belong to the FeFe and CoFe (Figure S3, profile B). After the etching, the shell thickness of the CoFe layer was reduced, and the signal of FeFe phase became thus detectable. The reason for forming the yolk-shell structure (instead of a shell-in-shell structure observed in Figure 1B-3) may be explained in the following way: Owing to the differences in the crystal structures between FeFe and CoFe, many defects exist at the interface between cores and shells. These interfaces become the softest parts, which can favor quick etching to allow the separation of the core and the shell to form a yolk-shell structure.

Other types of yolk-shell structure with different components could also be prepared by using core-shell NiCo@CoFe particles as the starting material (Figure S4). N_2 adsorption−desorption isotherms for yolk-shell and core-shell NiCo@CoFe particles had a drastic increase at low relative pressure (P/P_0 < 0.01). The yolk-shell particles exhibited much higher uptake in this range than the core-shell ones, indicating a larger accessible microporosity in the yolk-shell particles. In the range of P/P_0 = 0.4−1.0, the isotherms of the yolk-shell particles presented a hysteresis loop, while the core-shell particles did not, suggesting that a slight delay of desorption happened in the yolk-shell particles. The surface area of the yolk-shell particles was around 190 m^2/g, which was almost twice the value of that of the core-shell particles (100 m^2/g). In general, the NiCo shows a higher specific surface area than the CoFe. In the case of core-shell NiCo@CoFe particles, it is difficult for the N_2 molecules to enter the NiCo core region. In contrast, the yolk-shell NiCo@CoFe particles possessed thinner CoFe shells, so N_2 molecules could more easily pass through this thin shell and access the inner NiCo region with high uptake capability. For these reasons, the yolk-shell particles can have a higher accessible specific surface area than the core-shell particles.

3.3. PB Analogues with a Yolk-Double-Shell Structure.

As demonstrated in the two examples above, shell-in-shell and yolk-shell structures were achieved by crystal growth followed by chemical etching. Here, we used a hollow structure prepared by chemical etching as seeds for further crystal growth. The manner in which hollow particles perform as seeds was investigated. Unlike solid seeds, hollow seeds offer additional empty space inside the particles, providing good diffusion of guest species from the outside. It became possible to induce homogeneous nucleation and growth over the whole area of the hollow structure.

FeFe particles were first etched to prepare a hollow structure and then used as the seeds for the crystal growth of NiCo layers (Figure 4A). After the crystal growth, a yolk-shell structure with

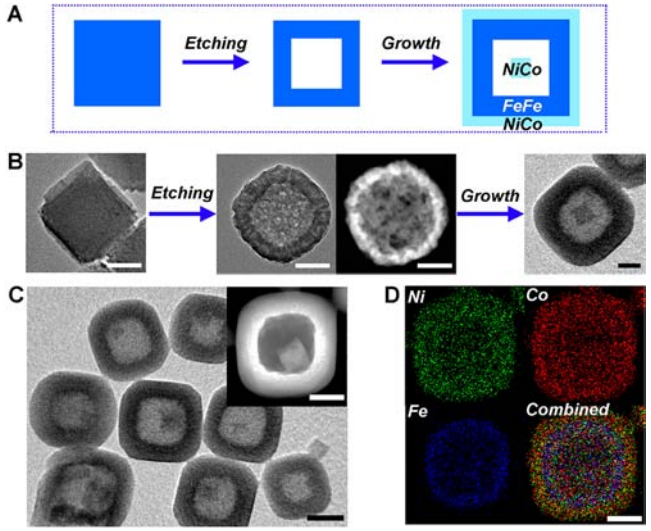

Figure 4. (A) Schematic illustration for making a yolk-double-shell particle. (B) TEM images of samples at different stages corresponding to the hypothesis shown in (A). (C) Low-magnified TEM image of NiCo@(FeFe@NiCo) particles with a yolk-double-shell structure and HAADF-STEM image of one selected particle. (D) Elemental mapping images of NiCo@(FeFe@NiCo) particles with a yolk-double-shell structure. All the scale bars are 100 nm.

double-layered shells was realized (Figure 4B). Almost all the particles had smooth surfaces and contained small nanoparticles inside the hollow cavity (Figure 4C). On the basis of elemental distribution, double-layered structures could be distinguished in the shell region (Figure 4D). The outer shell was NiCo, while the inner shell was FeFe. The small nanoparticles deposited inside the hollow cavity were NiCo. The wide-angle XRD pattern of the obtained particles demonstrated a pure *fcc* crystal structure, which matches typical PB analogues very well. The obtained yolk-double-shell structure was described as NiCo@(FeFe@NiCo). There were significant differences in N_2 adsorption−desorption behavior between yolk-double-shell and solid particles. In the case of NiCo@(FeFe@NiCo) particles, a large hysteresis loop was observed in the range of P/P_0 = 0.4−0.95. Unlike the hysteresis loop shown in Figure 2A, only one step was confirmed in the desorption isotherm (Figure 2B). The shell-in-shell hollow structure (shown in Figure 1) well served as barriers when the adsorbed molecules leave the interior cavity, thereby resulting in a large hysteresis loop. Thus, tuning hollow-based morphology can strongly affect the gas

dx.doi.org/10.1021/ja3096703 | J. Am. Chem. Soc. 2013, 135, 384−391

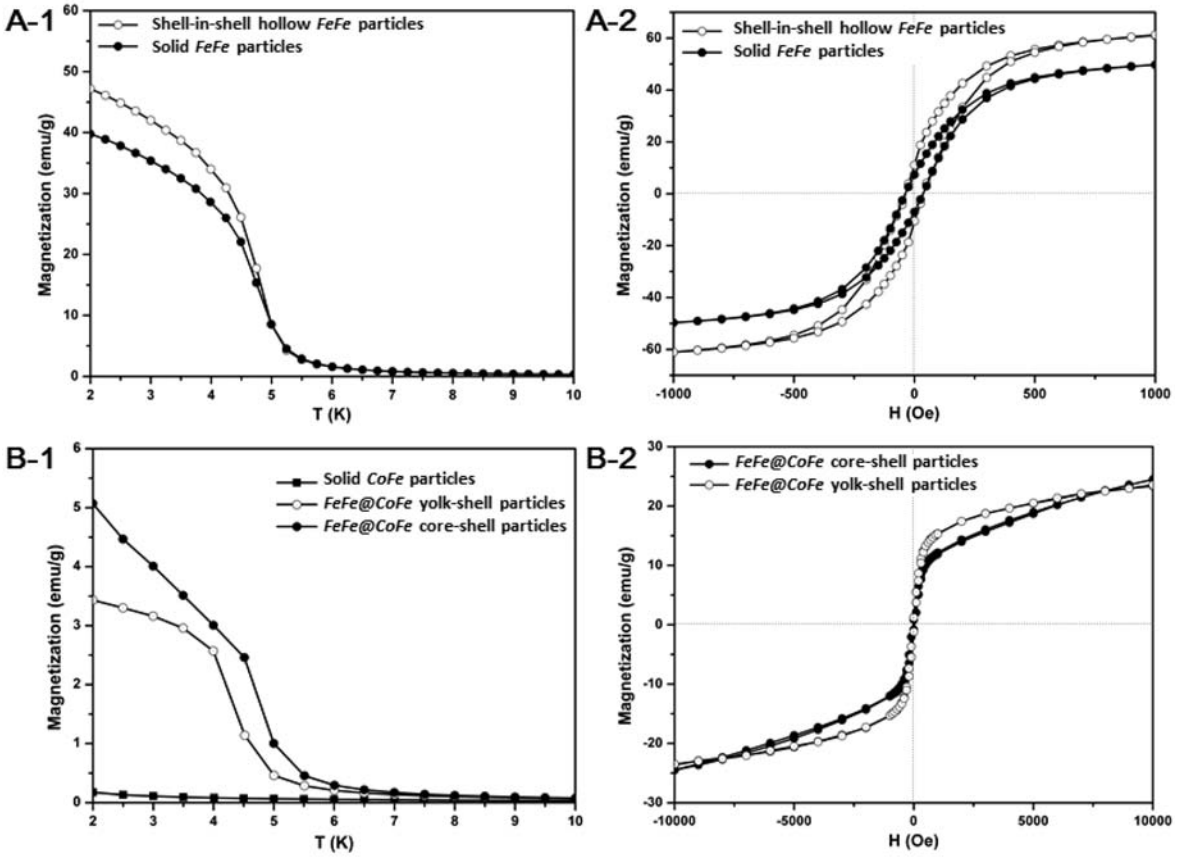

Figure 5. (A-1) Field-cooled magnetization curves shell-in-shell hollow FeFe particles and solid FeFe particles (H = 100 Oe). (A-2) Field-dependent magnetization curves of shell-in-shell hollow FeFe particles and solid FeFe particles at 2 K. (B-1) Field-cooled magnetization curves of FeFe@CoFe yolk-shell particles, FeFe@CoFe core-shell particles, and solid CoFe particles (H = 100 Oe). (B-2) Field-dependent magnetization curves of of FeFe@CoFe yolk-shell particles and FeFe@CoFe core-shell particles at 2 K.

adsorption−desorption behavior. The delayed guest molecule release might be applicable to the controlled release, in which slow release is essential, as it is with drug delivery.[65]

3.4. Magnetic Property of Hollow-Based PB Analogues. Cyanide-based coordination polymers, such as PB and PB analogues, are important and well-known magnetic materials.[48,50,53,54,56] Therefore, a thorough understanding of how hollow-based particles influence the magnetic property is important. A combination of heterocomponents into one composite can offer integrated functions, such as unique magnetic properties.[48,66] Figure 5A-1 shows field-cooled magnetization curves of shell-in-shell hollow FeFe particles and solid ones. Both samples showed similar magnetic ordering temperatures (T_c) around 5.5 K, indicating that the morphology did not affect the T_c of FeFe PB.[67] However, the saturated magnetization (M_s) of shell-in-shell hollow PB is higher than that of solid PB, according to the field-dependent magnetization curves recorded at 2 K (Figure 5A-2). The solid FeFe particles contained many defects that we called 'soft' parts. In the preparation of shell-in-shell hollow FeFe particles, the 'soft' parts were removed by etching. Therefore, the shell-in-shell hollow particles showed better crystallinity and fewer defects than the solid ones, as confirmed by the XRD profiles (Figure S1). Owing to the better crystallinity and fewer defects, the shell-in-shell hollow particles showed a higher M_s than the solid ones.

Other than shell-in-shell hollow particles with a single-component, yolk-shell and core-shell PB analogue particles with heterocomponents showed differences in magnetic properties. The FeFe@CoFe core-shell and yolk-shell particles showed ordering temperatures at around 5.5 and 6 K, respectively (Figure 5B-1), differently from the paramagnetic property of the CoFe itself. Such T_c was very close to the T_c of FeFe,[67] demonstrating that the magnetic property of PB analogues can be changed by the formation of composites. The T_c of the obtained composites followed one of the components,[58] in this case, close to FeFe. Although both FeFe@CoFe core-shell and yolk-shell particles showed a similar ordering temperature, the field-dependent magnetization process is totally different. Figure 5B-2 illustrates a quicker increase of magnetization of FeFe@CoFe yolk-shell particles from 0 to 6000 Oe. Considering that yolk-shell particles have thinner shells and smaller cores, the local magnetic moments in yolk-shell particles can be aligned more easily than those of core-shell particles, resulting in a quicker increase of magnetization in a low external field.[43] We may say that the existence of core can affect the ordering temperature, while the hollow structure can accelerate the magnetization of PB analogues. This example demonstrates that magnetization process can be designed by morphological control.

4. CONCLUSIONS

We established a new synthetic concept to prepare microporous CPs with multiple nanoarchitectures by sequentially controlling the growth and etching processes. By etching precursors with a heterogeneous distribution of defects, shell-

dx.doi.org/10.1021/ja3096703 | J. Am. Chem. Soc. 2013, 135, 384−391

in-shell hollow structures were obtained. By using core-shell precursors with various heterocompositions, yolk-shell structures were prepared. Furthermore, we demonstrated that hollow particles could be used as seed to obtain yolk-double-shell structures. The nitrogen gas sorption behavior of these microporous CPs with hollow-based structures was found to be significantly different from that of solid counterparts. Multiple hollow structures exhibited a much slower release in the desorption isotherms, which may be utilized in future applications requiring a slow release of guest molecules, such as drug delivery. In addition, our hollow-based structures could alternate their magnetic properties. Through this study, we strongly believe that our exquisite construction in CPs can be expected to be utilized in many other kinds of coordination polymers and improve the performance and range of applications.

■ ASSOCIATED CONTENT

Supporting Information

Detailed characterization data of wide-angle XRD measurement and SEM and TEM observation of shell-in-shell hollow FeFe, FeFe@CoFe core-shell, FeFe@CoFe yolk-shell, NiCo@CoFe yolk-shell, and NiCo@(FeFe@NiCo) particles with a yolk-double-shell structure. This information is available free of charge via the Internet at http://pubs.acs.org.

■ AUTHOR INFORMATION

Corresponding Author

Hu.Ming@nims.go.jp; Yamauchi.Yusuke@nims.go.jp

Notes

The authors declare no competing financial interest.

■ REFERENCES

(1) Yaghi, O. M.; O'Keeffe, M.; Ockwig, N. W.; Chae, H. K.; Eddaoudi, M.; Kim, J. *Nature* **2003**, *423*, 705−714.
(2) Kitagawa, S.; Kitaura, R.; Noro, S. *Angew. Chem., Int. Ed.* **2004**, *43*, 2334−2375.
(3) Horike, S.; Shimomura, S.; Kitagawa, S. *Nat. Chem.* **2009**, *1*, 695−704.
(4) Long, J. R.; Yaghi, O. M. *Chem. Soc. Rev.* **2009**, *38*, 1213−1214.
(5) Meek, S. T.; Greathouse, J. A.; Allendorf, M. D. *Adv. Mater.* **2011**, *23*, 249−267.
(6) Furukawa, H.; Kim, J.; Ockwig, N. W.; O'Keeffe, M.; Yaghi, O. M. *J. Am. Chem. Soc.* **2008**, *130*, 11650−11661.
(7) Furukawa, H.; Ko, N.; Go, Y. B.; Aratani, N.; Choi, S. B.; Choi, E.; Yazaydin, A. Ö.; Snurr, R. Q.; O'Keeffe, M.; Kim, J.; Yaghi, O. M. *Science* **2010**, *329*, 424−428.
(8) Furukawa, H.; Yaghi, O. M. *J. Am. Chem. Soc.* **2009**, *131*, 8875−8883.
(9) Jiang, H. L.; Tatsu, Y.; Lu, Z. H.; Xu, Q. *J. Am. Chem. Soc.* **2010**, *132*, 5586−5587.
(10) Lan, Y. Q.; Jiang, H. L.; Li, S. L.; Xu, Q. *Adv. Mater.* **2011**, *23*, 5015−5020.
(11) Zhao, X.; Xiao, B.; Fletcher, A. J.; Thomas, K. M.; Bradshaw, D.; Rosseinsky, M. J. *Science* **2004**, *306*, 1012−1015.
(12) Durand, P.; Fornasieri, G.; Baumier, C.; Beaunier, P.; Durand, D.; Rivière, E.; Bleuzen, A. *J. Mater. Chem.* **2010**, *20*, 9348−9354.
(13) Lu, G.; Farha, O. K.; Kreno, L. E.; Schoenecker, P. M.; Walton, K. S.; Duyne, R. P. V.; Hupp, J. T. *Adv. Mater.* **2011**, *23*, 4449−4452.
(14) Rieter, W. J.; Taylor, K. M. L.; An, H. Y.; Lin, W. L.; Lin, W. B. *J. Am. Chem. Soc.* **2006**, *128*, 9024−9025.
(15) Tanaka, D.; Henke, A.; Albrecht, K.; Moeller, M.; Nakagawa, K.; Kitagawa, S.; Groll, J. *Nat. Chem.* **2010**, *2*, 410−416.
(16) Uehara, H.; Diring, S.; Furukawa, S.; Kalay, Z.; Tsotsalas, M.; Nakahama, M.; Hirai, K.; Kondo, M.; Sakata, O.; Kitagawa, S. *J. Am. Chem. Soc.* **2011**, *133*, 11932−11935.
(17) Uemura, T.; Kitagawa, S. *J. Am. Chem. Soc.* **2003**, *125*, 7814−7815.
(18) Cravillon, J.; Nayuk, R.; Springer, S.; Feldhoff, A.; Huber, K.; Wiebcke, M. *Chem. Mater.* **2011**, *23*, 2130−2141.
(19) Li, P.; Z., Maeda, Y.; Xu, Q. *Chem. Commun.* **2011**, *47*, 8436−8438.
(20) Lin, W.; Rieter, W. J.; Taylor, K. M. *Angew. Chem., Int. Ed.* **2009**, *48*, 650−658.
(21) Puigmartí-Luis, J.; Rubio-Martínez, M.; Hartfelder, U.; Imaz, I.; Maspoch, D.; Dittrich, P. S. *J. Am. Chem. Soc.* **2011**, *133*, 4216−4219.
(22) Spokoyny, A. M.; Kim, D.; Sumrein, A.; Mirkin, C. A. *Chem. Soc. Rev.* **2009**, *38*, 1218−1227.
(23) Tsuruoka, T.; Furukawa, S.; Takashima, Y.; Yoshida, K.; Isoda, S.; Kitagawa, S. *Angew. Chem., Int. Ed.* **2009**, *48*, 4739−4743.
(24) Umemura, A.; Diring, S.; Furukawa, S.; Uehara, H.; Tsuruoka, T.; Kitagawa, S. *J. Am. Chem. Soc.* **2011**, *133*, 15506−15513.
(25) Vaucher, S.; Fielden, J.; Li, M.; Dujardin, E.; Mann, S. *Nano Lett.* **2002**, *2*, 225−229.
(26) Vaucher, S.; Li, M.; Mann, S. *Angew. Chem., Int. Ed.* **2000**, *39*, 1793−1796.
(27) Caruso, F.; Caruso, R. A.; Mohwald, H. *Science* **1998**, *282*, 1111−1114.
(28) Chen, J. Y.; Yang, M.; Zhang, Q.; Cho, E. C.; Cobley, C. M.; Kim, C.; Glaus, C.; Wang, L. V.; Welch, M. J.; Xia, Y. *Adv. Funct. Mater.* **2010**, *20*, 3684−3694.
(29) Lou, X. W.; Archer, L. A.; Yang, Z. C. *Adv. Mater.* **2008**, *20*, 3987−4019.
(30) Lou, X. W.; Li, C. M.; Archer, L. A. *Adv. Mater.* **2009**, *21*, 2536−2539.
(31) Lou, X. W.; Wang, Y.; Yuan, C. L.; Lee, J. Y.; Archer, L. A. *Adv. Mater.* **2006**, *18*, 2325−2329.
(32) Ma, Y. R.; Qi, L. M. *J. Colloid Interface Sci.* **2009**, *335*, 1−10.
(33) Piao, Y.; Kim, J.; Na, H. B.; Kim, D.; Baek, J. S.; Ko, M. K.; Lee, J. H.; Shokouhimehr, M.; Hyeon, T. *Nat. Mater.* **2008**, *7*, 242−247.
(34) Xia, Y. N.; Li, W.; Cobley, C. M.; Chen, J.; Xia, X.; Zhang, Q.; Yang, M.; Cho, E. C.; Brown, P. K. *Acc. Chem. Res.* **2011**, *44*, 914−924.
(35) Zhang, T. R.; Ge, J.; Hu, Y.; Zhang, Q.; Aloni, S.; Yin, Y. *Angew. Chem., Int. Ed.* **2008**, *47*, 5806−5811.
(36) Cheng, F. Y.; Ma, H.; Li, Y. M.; Chen, J. *Inorg. Chem.* **2007**, *46*, 788−794.
(37) Gonzalez, E.; Arbiol, J.; Puntes, V. F. *Science* **2011**, *334*, 1377−1380.
(38) (a) Lai, X. Y.; Li, J.; Korgel, B. A.; Dong, Z.; Li, Z.; Su, F.; Du, J.; Wang, D. *Angew. Chem., Int. Ed.* **2011**, *50*, 2738−2741. (b) Lee, I.; Joo, J. B.; Yin, Y.; Zaera, F. *Angew. Chem., Int. Ed.* **2011**, *50*, 10208−10211. (c) Liu, J.; Qiao, S. Z.; Hartono, S. B.; Lu, G. Q. *Angew. Chem., Int. Ed.* **2010**, *49*, 4981−4985. (d) Yang, Y.; Liu, X.; Li, X.; Zhao, J.; Bai, S.; Liu, J.; Yang, Q. *Angew. Chem., Int. Ed.* **2012**, *51*, 9164−9168. (e) Liu, J.; Qiao, S. Z.; Chen, J. S.; Lou, X. W.; Xing, X.; Lu, G. Q. *Chem. Commun.* **2011**, *47*, 12578−12591. (f) Yec, C. C.; Zeng, H. C. *Chem. Mater.* **2012**, *24*, 1917−1929. (g) Liu, N.; Wu, H.; McDowell, M. T.; Yao, Y.; Wang, C.; Cui, Y. *Nano Lett.* **2012**, *12*, 3315−3321.
(39) Xiong, S. L.; Zeng, H. C. *Angew. Chem., Int. Ed.* **2012**, *51*, 949−952.
(40) Xu, H. L.; Wang, W. Z. *Angew. Chem., Int. Ed.* **2007**, *46*, 1489−1492.
(41) Yu, J. G.; Yu, H. G.; Guo, H. T.; Li, M.; Mann, S. *Small* **2008**, *4*, 87−91.
(42) Ameloot, R.; Vermoortele, F.; Vanhove, W.; Roeffaers, M. B. J.; Sels, B. F.; Vos, D. E. D. *Nat. Chem.* **2011**, *3*, 382−387.
(43) Hu, M.; Furukawa, S.; Ohtani, R.; Sukegawa, H.; Nemot, Y.; Reboul, J.; Kitagawa, S.; Yamauchi, Y. *Angew. Chem., Int. Ed.* **2012**, *51*, 984−988.
(44) Huo, J.; Wang, L.; Irran, E.; Yu, H.; Gao, J.; Fan, D.; Li, B.; Wang, J.; Ding, W.; Amin, A. M.; Li, C.; Ma, L. *Angew. Chem., Int. Ed.* **2010**, *49*, 9237−9241.

(45) Lee, H. J.; Cho, W.; Oh, M. *Chem. Commun.* **2012**, *48*, 221−223.
(46) McHale, R.; Ghasdian, N.; Liu, Y.; Ward, M. B.; Hondow, N. S.; Wang, H.; Miao, Y.; Brydson, R.; Wang, X. *Chem. Commun.* **2010**, *46*, 4574−4576.
(47) Roy, X.; Hui, J. K. H.; Rabnawaz, M.; Liu, G. J.; MacLachlan, M. J. *J. Am. Chem. Soc.* **2011**, *133*, 8420−8423.
(48) Dechambenoit, P.; Long, J. R. *Chem. Soc. Rev.* **2011**, *40*, 3249−3265.
(49) DeLongchamp, D. M.; Hammond, P. T. *Adv. Funct. Mater.* **2004**, *14*, 224−232.
(50) Ferlay, S.; Mallah, T.; Ouahes, R.; Veillet, P.; Verdaguer, M. *Nature* **1995**, *378*, 701−703.
(51) Kaye, S. S.; Long, J. R. *J. Am. Chem. Soc.* **2005**, *127*, 6506−6507.
(52) Neff, V. D. *J. Electrochem. Soc.* **1985**, *132*, 1382−1384.
(53) Ohkoshi, S.; Abe, Y.; Fujishima, A.; Hashimoto, K. *Phys. Rev. Lett.* **1999**, *82*, 1285−1288.
(54) Pejakovic, D. A.; Manson, J. L.; Miller, J. S.; Epstein, A. J. *Phys. Rev. Lett.* **2000**, *85*, 1994−1997.
(55) Ricci, F.; Palleschi, G. *Biosens. Bioelectron.* **2005**, *21*, 389−407.
(56) Sato, O.; Iyoda, T.; Fujishima, A.; Hashimoto, K. *Science* **1996**, *272*, 704−705.
(57) Catala, L.; Brinzei, D.; Prado, Y.; Gloter, A.; Stéphan, O.; Rogez, G.; Mallah, T. *Angew. Chem., Int. Ed.* **2009**, *48*, 183−187.
(58) Dumont, M. F.; Knowles, E. S.; Guiet, A.; Pajerowski, D. M.; Gomez, A.; Kycia, S. W.; Weisel, M. W.; Talham, D. R. *Inorg. Chem.* **2011**, *50*, 4295−4300.
(59) Presle, M.; Lemainque, J.; Guigner, J. M.; Larquet, E.; Maurin, I.; Boilot, J. P.; Gacoin, T. *New J. Chem.* **2011**, *35*, 1296−1301.
(60) Ming, H.; Torad, N. L. K.; Chiang, Y. D.; Wu, K. C. W.; Yamauchi, Y. *CrystEngComm* **2012**, *14*, 3387−3396.
(61) Pajerowski, D. M.; Andrus, M. J.; Gardner, J. E.; Knowles, E. S.; Meisel, M. W.; Talham, D. R. *J. Am. Chem. Soc.* **2010**, *132*, 4058−4059.
(62) Kotsakis, N.; Raptopoulou, C. P.; Tangoulis, V.; Terzis, A.; Giapintzakis, J.; Jakusch, T.; Kiss, T.; Salifoglou, A. *Inorg. Chem.* **2003**, *42*, 22−31.
(63) Matzapetakis, M.; Karligiano, N.; Bino, A.; Dakanali, M.; Raptopoulou, C. P.; Tagoulis, V.; Terzis, A.; Giapintzakis, J.; Salifoglou, A. *Inorg. Chem.* **2000**, *39*, 4044−4051.
(64) Strouse, J.; Layten, S. W.; Strouse, C. E. *J. Am. Chem. Soc.* **1977**, *99*, 562−572.
(65) Horcajada, P.; Chalati, T.; Serre, C.; Gillet, B.; Sebrie, C.; Baati, T.; Eubank, J. F.; Heurtaux, D.; Clayette, P.; Kreuz, C.; Chang, J. S.; Hwang, Y. K.; Marsaud, V.; Bories, P. N.; Cynober, L.; Gil, S.; Férey, G.; Couvreur, P.; Gref, R. *Nat. Mater.* **2010**, *9*, 172−178.
(66) Madaeni, S. S.; Enayati, E.; Vatanpour, V. *Polymers Adv. Technol.* **2011**, *22*, 2556−256.
(67) Herren, F.; Fischer, P.; Ludi, A.; Halg, W. *Inorg. Chem.* **1980**, *19*, 956−959.